Plant Physiology®

Research Article

Transcription factor WOX11 modulates tolerance to cyst nematodes via adventitious lateral root formation

Jaap-Jan Willig [ID],[1,†] Nina Guarneri [ID],[1,†] Thomas van Loon [ID],[1] Sri Wahyuni [ID],[1]
Ivan E. Astudillo-Estévez [ID],[1,‡] Lin Xu [ID],[2] Viola Willemsen [ID],[3] Aska Goverse [ID],[1] Mark G. Sterken [ID],[1]
José L. Lozano-Torres [ID],[1] Jaap Bakker [ID][1] and Geert Smant [ID][1,*]

1   Laboratory of Nematology, Wageningen University & Research, Wageningen 6708 PB, The Netherlands
2   National Key Laboratory of Plant Molecular Genetics, CAS Center for Excellence in Molecular Plant Sciences, Institute of Plant Physiology and Ecology, Chinese Academy of Sciences, Shanghai 200032, China
3   Cluster of Plant Developmental Biology, Cell and Developmental Biology, Wageningen University & Research, Wageningen 6708 PB, The Netherlands

*Author for correspondence: geert.smant@wur.nl
†These authors contributed equally.
‡Present address: Instituto de Microbiología, Universidad San Francisco de Quito, Quito, Ecuador.
The author responsible for distribution of materials integral to the findings presented in this article in accordance with the policy described in the Instructions for Authors (https://academic.oup.com/plphys/pages/General-Instructions) is: Geert Smant.

Abstract

The transcription factor WUSCHEL-RELATED HOMEOBOX 11 (WOX11) in Arabidopsis (Arabidopsis thaliana) initiates the formation of adventitious lateral roots upon mechanical injury in primary roots. Root-invading nematodes also induce de novo root organogenesis leading to excessive root branching, but it is not known if this symptom of disease involves mediation by WOX11 and if it benefits the plant. Here, we show with targeted transcriptional repression and reporter gene analyses in Arabidopsis that the beet cyst nematode Heterodera schachtii activates WOX11-mediated adventitious lateral rooting from primary roots close to infection sites. The activation of WOX11 in nematode-infected roots occurs downstream of jasmonic acid-dependent damage signaling via ETHYLENE RESPONSE FACTOR109, linking adventitious lateral root formation to nematode damage to host tissues. By measuring different root system components, we found that WOX11-mediated formation of adventitious lateral roots compensates for nematode-induced inhibition of primary root growth. Our observations further demonstrate that WOX11-mediated rooting reduces the impact of nematode infections on aboveground plant development and growth. Altogether, we conclude that the transcriptional regulation by WOX11 modulates root system plasticity under biotic stress, which is one of the key mechanisms underlying the tolerance of Arabidopsis to cyst nematode infections.

Introduction

Soil-borne infections by cyst nematodes affect aboveground and belowground plant development and growth, sometimes resulting in large yield losses in agriculture (Jones et al. 2013). Biotic stress induced by cyst nematodes in the roots of host plants occurs at different stages of their infection cycle. Firstly, the infective second-stage juveniles (J2s) invade host roots and migrate intracellularly through the epidermis and cortex, causing extensive damage to root tissue. Secondly, after becoming sedentary, cyst nematodes take up large amounts of plant assimilates during feeding from modified plant cells, which therefore develop strong metabolic sink activity (Gheysen and Mitchum 2011; Jones et al. 2013; Bebber et al. 2014). As a response to nematode infections, plants remodel their root system by forming additional secondary roots (Goverse et al. 2000; Olmo et al. 2020;

Open Access

Willig et al. 2022; Guarneri et al. 2023). The de novo formation of secondary roots in response to endoparasitism by nematodes might be a mechanism to compensate for primary root growth inhibition caused by nematode infection (Guarneri et al. 2023). However, whether such a form of root system plasticity contributes to overall plant tolerance to cyst nematode infections remains to be investigated.

Depending on where and how secondary roots are formed, they are either classified as lateral roots or adventitious lateral roots (Sheng et al. 2017). During postembryonic development in *Arabidopsis* (*Arabidopsis thaliana*), periodic oscillations of auxin maxima at the root tip prime cells to form lateral roots that emerge in a regular acropetal pattern from the growing primary root (Fukaki and Tasaka 2009; van den Berg et al. 2016). The emergence of lateral roots is controlled by AUXIN RESPONSE FACTOR7 (ARF7) and ARF19, which directly regulate *LATERAL ORGAN BOUNDARIES DOMAIN16* (*LBD16*) and other *LBD* genes (Okushima et al. 2007). In contrast, adventitious lateral roots do not follow an acropetal pattern as they emerge in between and opposite of existing lateral roots. Moreover, adventitious lateral roots emerge in response to tissue damage, and their formation is regulated by a separate pathway mediated by the transcription factor WUSCHEL-RELATED HOMEOBOX11 (WOX11) (Liu et al. 2014; Hu and Xu 2016; Sheng et al. 2017). After cutting the primary root, local accumulation of auxin activates WOX11 transcriptional activity through auxin response elements in its promotor region (Liu et al. 2014). Subsequently, WOX11 induces the expression of *LBD16* but also the expression of other *WOX* genes (Hu and Xu 2016; Sheng et al. 2017). Ultimately, this leads to the de novo formation of secondary roots close to the injury site (Cai et al. 2014; Liu et al. 2014; Hu and Xu 2016; Sheng et al. 2017). Cyst nematode infection in primary roots of *Arabidopsis* triggers the formation of secondary roots, which does not follow an acropetal patterning (Guarneri et al. 2022). Instead, secondary roots often form clusters at nematode infection sites. As to whether the formation of these secondary roots depends on the WOX11-mediated pathway and whether they should thus be classified as adventitious lateral roots is still a knowledge gap.

We have recently demonstrated that the formation of secondary roots near nematode infection sites involves damage-induced jasmonic acid (JA) signaling (Guarneri et al. 2023). Tissue damage caused by intracellular migration of infective juveniles of *Heterodera schachtii* induces the biosynthesis of JA, which activates the transcription factor ETHYLENE RESPONSE FACTOR (ERF)109 via the JA receptor CORONATINE INSENSITIVE (COI)1. ERF109, in turn, can trigger local biosynthesis of auxin by directly binding to the promoters of auxin biosynthesis genes *ASA1* and *YUC2* (Cai et al. 2014). Indeed, our data showed that COI1/ERF109-mediated formation of secondary roots from nematode-infected primary roots depends on local biosynthesis and accumulation of auxin (Guarneri et al. 2023). WOX11-mediated formation of adventitious lateral roots upon root injury also involves

local accumulation of auxin (Liu et al. 2014). However, it remains to be demonstrated if WOX11 becomes activated by COI1- and ERF109-mediated damage signaling in nematode-infected roots.

Several recent reports in the literature point at a role for WOX11-mediated root plasticity in modulating plant responses to abiotic stresses. For instance, WOX11, designated as PagWOX11/WOX12a, in poplar (*Populus*) mediates changes in root system architecture in response to drought and salt stress (Wang et al. 2020, 2021). Overexpression and dominant repression of the *WOX11* gene in poplar plants alters the number of adventitious roots formed under high saline conditions (Liu et al. 2022). Likewise, the loss-of-function mutant *wox11* in rice (*Oryza sativa*) exhibits reduced root system development in response to drought as compared to wild-type plants (Cheng et al. 2016). Based on these findings, WOX11-mediated root plasticity is thought to enhance plant tolerance to abiotic stress. However, whether WOX11-mediated root plasticity is also involved in mitigating the impact of biotic stresses on the root system is not known.

In this study, we first addressed whether cyst nematode-induced secondary roots qualify as damage-induced adventitious lateral roots. Hereto, we monitored de novo secondary root formation in *Arabidopsis* seedlings of the double mutant *arf7/arf19* and the WOX11 transcriptional repressor mutant *35S:WOX11-SRDX* in the *arf7/arf19* background (Hiratsu et al. 2003) infected with *H. schachtii*. Second, we asked whether the regulation of *WOX11* in nematode-infected *Arabidopsis* roots occurs downstream of JA-dependent damage signaling through COI1 and ERF109. To answer this question, we performed a time course experiment measuring *pWOX11::GFP* expression with confocal microscopy in wild-type seedlings and *coi1-2* and *erf109* mutant seedlings infected with *H. schachtii*. Third, we assessed if WOX-11-mediated root system plasticity compensates for the inhibition of primary root growth upon cyst nematode infection. For this, we measured different components of the root system architecture of nematode-infected WOX11 transcriptional repressor mutant and wild-type *Arabidopsis* plants. Last, we tested if WOX11-mediated root system plasticity contributes to the overall tolerance of *Arabidopsis* to cyst nematode infections. To this end, we compared the aboveground plant growth and development of cyst nematode-infected *35S:WOX11-SRDX* mutants and wild-type *Arabidopsis* for a period of 3 wk after inoculation. Based on our data, we propose a model wherein the formation of WOX11-mediated adventitious lateral roots enhances the tolerance of *Arabidopsis* to biotic stress by cyst nematode infections.

Results

Cyst nematodes induce the formation of adventitious lateral roots

Our earlier work showed that *H. schachtii* induces the de novo formation of secondary roots between or across fully developed lateral roots near nematode infection sites
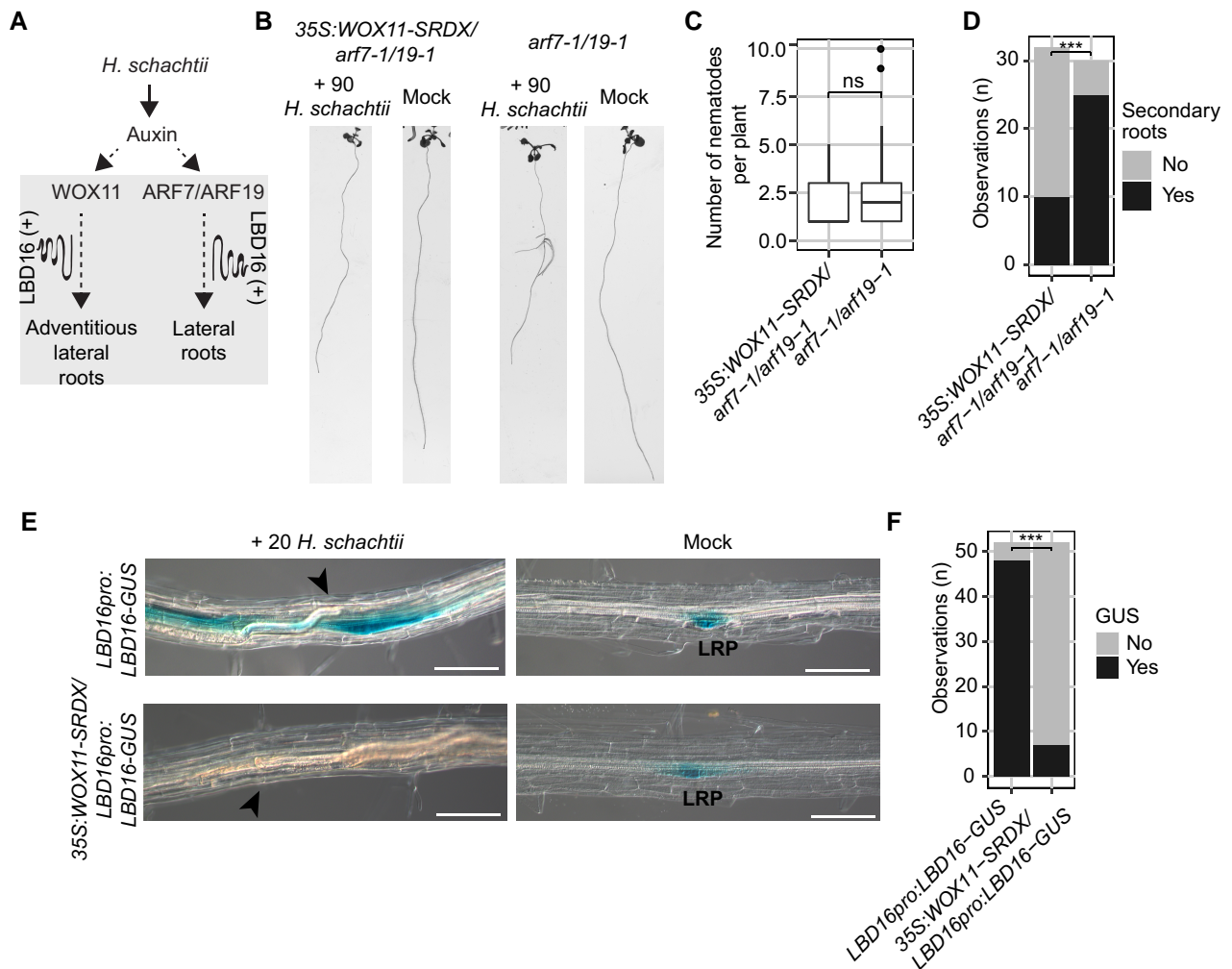
Figure 1. *H. schachtii* induces adventitious lateral root formation in a WOX11- and LBD16-dependent manner. **A)** Schematic diagram of *H. schachtii*- and WOX11-mediated adventitious lateral root emergence. Highlighted area indicates the tested part of the pathway. Curling line and "+" indicate the involvement of multiple proteins, including LBD16. **B to D)** Seven-day-old *35S:WOX11-SRDX/arf7-1/19-1* and *arf7-1/arf19-1* mutant seedlings were inoculated with 90 *H. schachtii* juveniles or with mock solution. At 7 dpi, scans were made of the root system. **B)** Representative pictures of *35S:WOX11-SRDX/arf7-1/19-1* and *arf7-1/arf19-1* mutant seedlings inoculated with 90 *H. schachtii* or with mock solution. **C)** Number of juveniles that invaded the primary roots. For boxplots, the horizontal line represents the median, the whiskers indicate the maximum/minimum range, and the black dots represent the outliers (1.5 times the interquartile range). The significance of differences between genotypes was calculated by an unpaired 2-sample Wilcoxon test, ns = not significant (*n* = 30 to 32). **D)** Number of seedlings that show secondary roots (yes) that are associated with *H. schachtii* infection sites or no secondary roots at all (no). Data from 3 independent biological repeats of the experiment was combined. Statistical significance was calculated by a Pairwise Z-test *n* = 30 to 32; ***P < 0.001). **E, F)** Four-day-old *Arabidopsis* seedlings expressing the *LBD16pro:LBD16-GUS* and *35S:WOX11-SRDX/LBD16pro:LBD16-GUS* reporters were inoculated with 20 *H. schachtii* juveniles. At 4 dpi, GUS expression was stained for 3 h and seedlings were imaged. **E)** *LBD16pro:LBD16-GUS* and *35S:WOX11-SRDX/LBD16pro:LBD16-GUS* expression at nematode infection sites in roots. Black arrowheads indicate the nematode head. LRP indicates lateral root primordia. Scale bar = 100 μm. **F)** Number of observations with (yes) or without (no) GUS staining at the nematode infection site in roots of wild-type Col-0 seedlings. Data from 3 independent biological repeats of the experiment were combined. Statistical significance was calculated by a Pairwise Z-test *n* = 52 and ***P < 0.001.

(Guarneri et al. 2023). Here, we hypothesized that these secondary roots are adventitious lateral roots, the formation of which depends on WOX11-mediated transcriptional regulation (Fig. 1A). To test this hypothesis, we inoculated *H. schachtii* on the lateral root-deficient *arf7-1/19-1* double mutant, which is unable to form acropetal lateral roots, and the transcription repressor mutant *35S:WOX11-SRDX/arf7-1/19-1* (Hiratsu et al. 2003), which is unable to form

neither acropetal nor adventitious lateral roots (Fig. 1, B to D). Importantly, we observed no difference in the number of nematodes per plant between *arf7-1/19-1* and *35S:WOX11-SRDX/arf7-1/19-1* (Fig. 1C), indicating that both *Arabidopsis* lines were exposed to similar levels of biotic stress. However, significantly fewer *35S:WOX11-SRDX/arf7-1/19-1* plants showed secondary root formation upon inoculation with *H. schachtii* inoculation compared to *arf7-1/19-1*
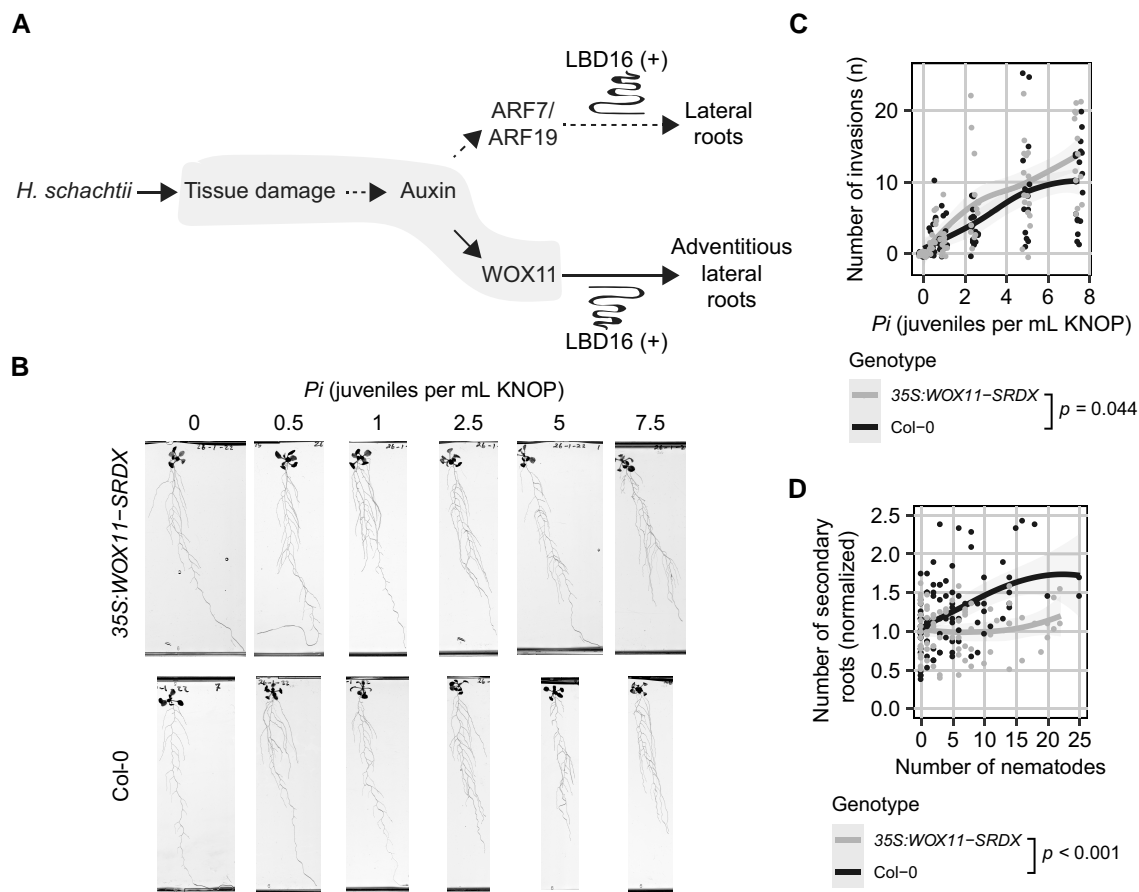
Figure 2. WOX11 is required in *H. schachtii*-induced adventitious lateral root formation in a density-dependent manner. **A)** Schematic diagram of *H. schachtii*- and WOX11-mediated adventitious lateral roots emergence. Highlighted area indicates the tested part of the pathway. Curling line and "+" indicate the involvement of multiple proteins, including LBD16. **B to D)** Nine-day-old *35S:WOX11-SRDX* and wild-type Col-0 seedlings were inoculated with nematode densities (P_i) ranging from 0 to 7.5 *H. schachtii* J2s (mL modified KNOP media). Roots were scanned and nematodes were counted after acid fuchsin staining at 7 dpi. **B)** Representative images of *Arabidopsis* root systems at 7 dpi. **C)** Number of nematodes that successfully penetrated the roots per plant. **D)** Secondary roots formed per number of nematodes inside the roots. The total number of secondary roots of infected seedlings was normalized to the median respective component in mock-inoculated roots. Data from 2 independent biological repeats of the experiment were combined. The significance of differences between genotypes was calculated by analysis of variance ($n = 14$ to 18). Gray area indicates the 95% CI. Threshold for significance $P < 0.05$.

mutant plants (Fig. 1, B and D; Supplementary Fig. S1). From this, we concluded that the induction of secondary roots by *H. schachtii* is mediated by WOX11 and that these secondary roots therefore qualify as adventitious lateral roots.

WOX11-mediated formation of adventitious lateral roots from primary roots of *Arabidopsis* involves the downstream transcriptional activation of *LBD16* (Fig. 1A) (Sheng et al. 2017). To test if WOX11 activates *LBD16* in nematode-infected *Arabidopsis* roots, we monitored the expression of *LBD16* fused to *GUS* in wild-type (*LBD16pro:LBD16-GUS*) and *35S:WOX11-SRDX* (*35S:WOX11-SRDX/LBD16pro:LBD16-GUS*) seedlings inoculated with *H. schachtii* (Fig. 1, E and F). We found that *LBD16* was highly expressed in nematode infection sites in the wild type, but not in the *35S:WOX11-SRDX* background. This demonstrates that *H. schachtii* activates *LBD16* expression in a WOX11-dependent manner. Based on these observations, we concluded that cyst nematode

infections activate the WOX11/LBD16-mediated pathway to form adventitious lateral roots from primary roots.

Emergence of adventitious lateral roots associates with damage in primary roots

Previously, we showed that increasing nematode inoculation densities result in more tissue damage in *Arabidopsis* leading to a higher number of secondary roots emerging from infected primary roots (Guarneri et al. 2023). To test the hypothesis that WOX11 mediates this quantitative relationship between inoculation density and the number of secondary roots emerging from cyst nematode-infected primary roots (Fig. 2A), we inoculated 9-d-old seedlings of *35S:WOX11-SRDX* and wild-type plants with increasing densities of *H. schachtii* (Fig. 2B). At 7 days post-inoculation (dpi), the number of nematodes that had successfully penetrated the

roots was counted after staining with acid fuchsin (Fig. 2C). The number of infective juveniles in *35S:WOX11-SRDX* plants by inoculation density was significantly higher compared to wild-type Col-0 plants. This indicates that the transcriptional regulation by WOX11 in wild-type *Arabidopsis* plants reduces susceptibility to penetration by *H. schachtii*. Next, we counted the number of secondary roots to determine whether this corresponds with the number of nematodes inside the roots. It should be noted that uninfected *35S:WOX11-SRDX* plants have more secondary roots than wild-type Col-0 plants (Supplementary Fig. S2). To correct for this background effect of the SRDX-transcriptional repressor construct on root system architecture, we normalized the total number of secondary roots in infected seedlings to the average respective number in uninfected seedlings (Fig. 2D). As expected, after normalization, the number of secondary roots emerging from primary roots increased with the number of successful invasions of *H. schachtii* in wild-type *Arabidopsis*. However, no such association was observed in *35S:WOX11-SRDX* plants. We, therefore, concluded that the density-dependent adaptations in root system architecture to increasing levels of damage in nematode-infected roots are brought about by WOX11-mediated formation of adventitious lateral roots.

COI1 and ERF109 modulate damage-induced activation of *WOX11* at nematode infection sites

De novo formation of secondary roots on nematode-infected primary roots of *Arabidopsis* is mediated by damage-induced activation of JA signaling via COI1 and ERF109 (Guarneri et al. 2023). In this study, we tested whether COI1 and ERF109 are required for the regulation of *WOX11* in nematode infection sites (Fig. 3A). Hereto, we imaged nucleus-localized *pWOX11::GFP* expression within single-nematode infection sites in the *coi1-2* and *erf109* mutants and wild-type Col-0 at 2, 3, 4, and 7 dpi (Fig. 3; Supplementary Fig. S3). Cyst nematode infection typically causes tissue autofluorescence in *Arabidopsis* roots (Hoth et al. 2005). To filter out this autofluorescence from the fluorescent signal emitted by the GFP construct, we subtracted a Gaussian blurred image from the original images (Supplementary Fig. S4). Hereafter, we observed a gradual increase in the *pWOX11::GFP*-derived fluorescent signal in nematode infection sites over time in *coi1-2*, *erf109*, and wild-type Col-0 (Supplementary Fig. S3, A to F), with wild-type Col-0 showing the strongest increase (Supplementary Fig. S3F). For instance, at 4 dpi, wild-type Col-0 plants showed significantly more nuclear GFP fluorescence in and around nematode feeding sites compared to *coi1-2* and *erf109* in the processed images (Fig. 3, B to D). We, therefore, concluded that 2 key components of the damage-induced JA signaling pathway, COI1 and ERF109, modulate *WOX11* expression in infection sites of *H. schachtii* in *Arabidopsis*.

Formation of adventitious lateral roots compensates for nematode-induced primary root growth inhibition

Next, we asked whether WOX11-mediated adventitious lateral root formation compensates for the inhibition of primary root growth due to nematode infections (Fig. 4A). To this end, we quantified root system architecture components (i.e. total root length, primary root length, total secondary root length, and average secondary root length) of nematode-infected roots of both *35S:WOX11-SRDX* and wild-type Col-0 plants (Fig. 2). Initially, we noticed that our measurements of root system architecture components followed a parabolic function with the minimum values at the infection rate of 15 juveniles per root, suggesting the existence of 2 density-dependent counteracting mechanisms (Supplementary Fig. S5). We, therefore, analyzed our data for the lower (Fig. 4) and higher infection rates separately (Supplementary Fig. S5). For plants infected with 0 to 15 juveniles per root, we found that the total root length was significantly more reduced by nematode infection in *35S: WOX11-SRDX* mutant plants than in wild-type Col-0 plants (Fig. 4, B and D). Interestingly, the growth of the primary root was not different between *35S:WOX11-SRDX* mutant plants and wild-type plants upon infection with cyst nematodes (Fig. 4C). However, the total length of the secondary roots of nematode-infected *35S:WOX11-SRDX* mutant plants was significantly smaller as compared to wild-type Col-0 plants (Fig. 4D). As the average secondary root length did not significantly differ between *35S:WOX11-SRDX* and wild-type *Arabidopsis* plants, WOX11 affects the root system architecture by increasing the number of secondary roots but not by extending secondary root growth (Supplementary Fig. S5E). For plants infected with 15 to 25 juveniles per plant, we observed no significant differences for the total root length (Supplementary Fig. S5B) between wild-type Col-0 and *35S: WOX11-SRDX*. Likewise, we found no differences in the primary root length (Supplementary Fig. S5C), total secondary root length (Supplementary Fig. S5D), and average secondary root length (Supplementary Fig. S5E). Based on our analyses, we concluded that WOX11-mediated formation of adventitious lateral roots compensates for nematode-induced inhibition of primary root growth at lower infection rates.

WOX11 modulates tolerance to cyst nematode infections

The growth of the green canopy area over time reflects the tolerance of *Arabidopsis* to biotic stress by root-feeding cyst nematodes (Willig et al. 2023). To assess if WOX11-mediated de novo formation of adventitious lateral roots modulates the tolerance of *Arabidopsis* to cyst nematode infection, we monitored the growth of the green canopy area of *35S:WOX11-SRDX* mutant and wild-type Col-0 seedlings for a period of 21 d after inoculation with different numbers of *H. schachtii* (Fig. 5, A and B). At the end of the experiment, the green canopy area of the *35S:WOX11-SRDX* mutant was smaller at higher inoculation densities of *H. schachtii* as compared to that of wild-type Col-0 plants (Fig. 5, C and D). Notably, the first significant reduction in green canopy area of *35S:WOX11-SRDX* plants by nematode infection was observed at inoculation densities between P_i
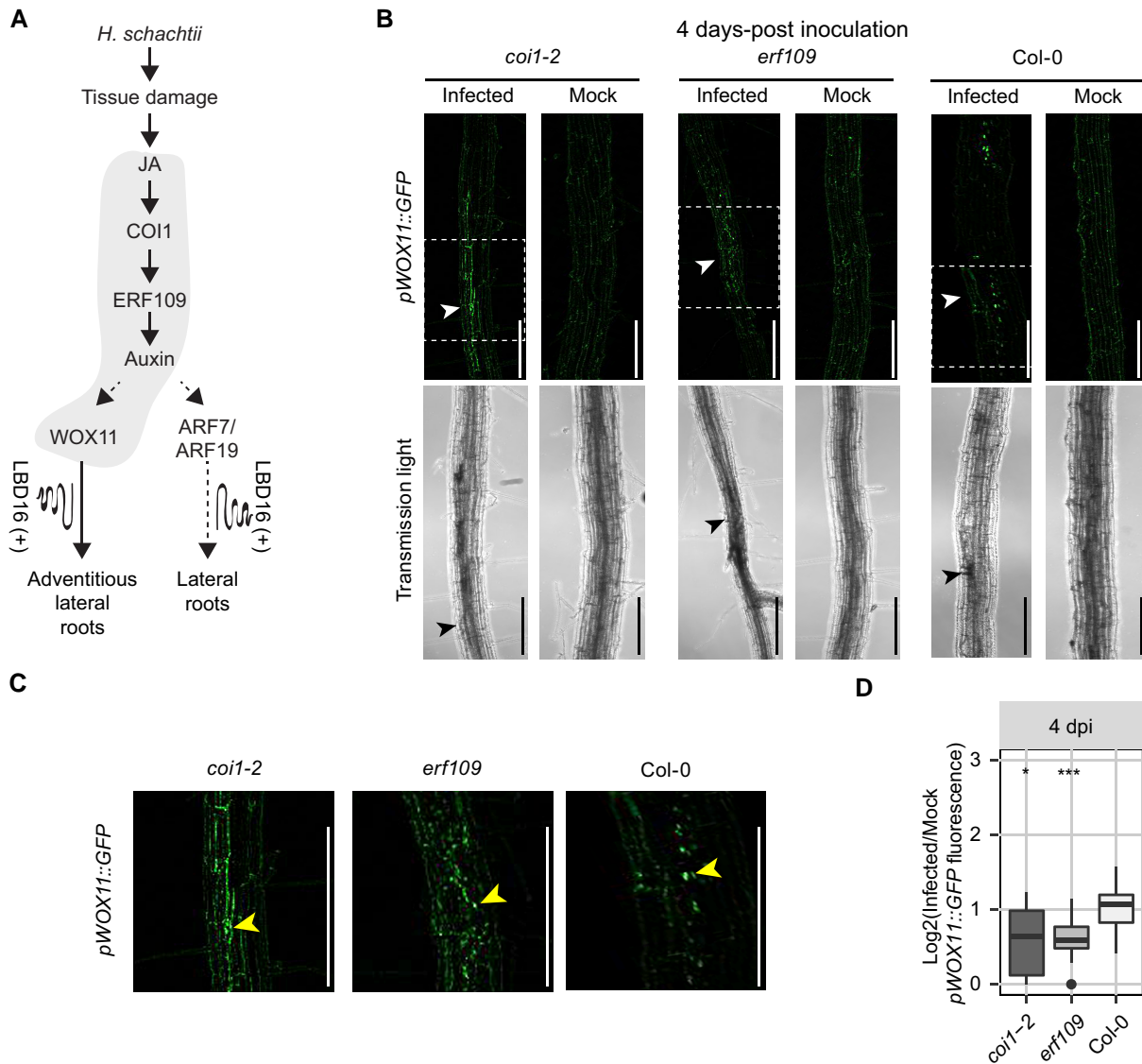
Figure 3. COI1 and ERF109 modulate *WOX11* expression upon *H. schachtii* infection. **A)** Schematic diagram of *H. schachtii*- and WOX11-mediated adventitious lateral root emergence. Highlighted area indicates the tested part of the pathway. Curling line and "+" indicate the involvement of multiple proteins, including LBD16. **B, C)** Four-day-old *Arabidopsis* seedlings were either inoculated with 10 *H. schachtii* second-stage juveniles (J2s) or with mock solution. At 4 dpi, seedlings were mounted in water and then imaged using a fluorescent confocal microscope. Single-nematode infection sites were selected for observation. Images are original. **B)** Representative pictures of infected and mock-inoculated seedlings expressing the *pWOX11::GFP* construct with nuclear localization signal in either wild-type Col-0, mutant *coi1-2*, or mutant *erf109* background at 4 dpi. To make the fluorescence more visible, the brightness was enhanced for all the representative pictures in the same way. **C)** Zoomed parts of the original image fluorescent signal that are indicated by dashed white box in **B)**. Yellow arrowhead indicates true fluorescent signal of *pWOX11::GFP* in the nucleus. **D)** Quantification of *pWOX11::GFP* fluorescent intensity induced by infection in wild-type Col-0, *coi1-2*, and *erf109* roots. Values represent log$_2$ of the fluorescence ratio between the GFP integrated density of infected and noninfected roots. For boxplots, the horizontal line represents the median, the whiskers indicate the maximum/minimum range, and the black dots represent the outliers (1.5 times the interquartile range). Scale bar: 200 μm. Data from 3 independent biological repeats of the experiment were combined. The significance of differences between fluorescent intensities in Co-0, *coi1-2*, and *erf109* per time point was calculated by a Wilcoxon rank sum test. ns = not significant, *$P < 0.05$, **$P < 0.01$, and ***$P < 0.001$ ($n = 15$).

2.5 and 5 J2s per gram sand, while in wild-type Col-0 plants, we observed a first significant reduction in green canopy area at P_i 7.5 J2s per gram sand. To quantify more exactly the difference in tolerance of *35S:WOX11-SRDX* and wild-type Col-0 plants, we fitted the growth rates of individual plants (Supplementary Figs. S6 and S7) to a logistic growth model. From this, we calculated the maximum projected green canopy area and determined the tolerance limit with 95% confidence interval (CI) (Fig. 5E). The relationship between maximum canopy area K and the P_i fitted a Gaussian curve,
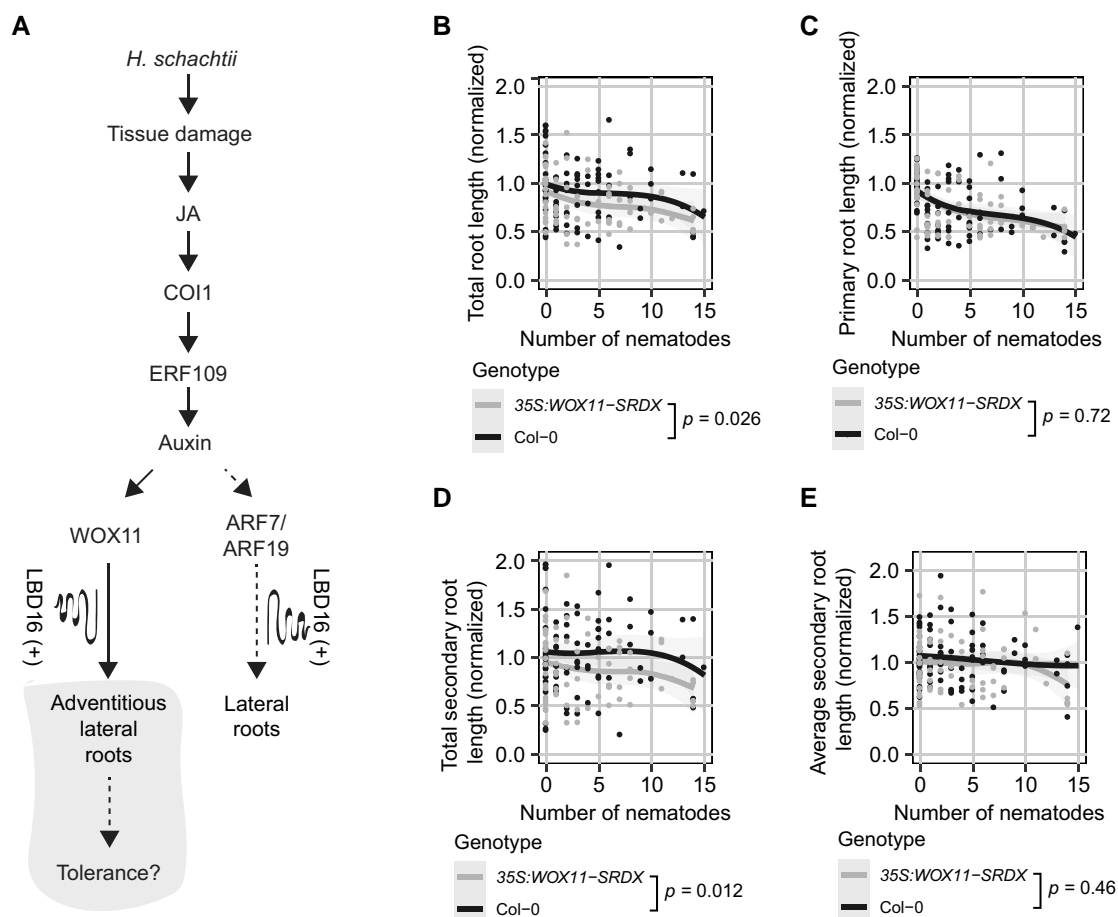
Figure 4. Formation of adventitious lateral roots compensates for nematode-induced primary root growth inhibition. **A)** Schematic diagram of *H. schachtii-* and WOX11-mediated adventitious lateral root emergence. Highlighted area indicates the tested part of the pathway. Curling line and "+" indicate the involvement of multiple proteins, including LBD16. **B to D)** Nine-day-old *35S:WOX11-SRDX* and wild-type Col-0 seedlings were inoculated densities (P_i) ranging from 0 to 7.5 *H. schachtii* J2s (mL modified KNOP media). Roots were scanned and nematodes were counted after fuchsine staining at 7 dpi. Root architectural components of infected seedlings were normalized to the median respective component in mock-treated roots. Data of 2 independent biological repeats of the experiment was combined. **B)** Total root length per number of nematodes inside the roots. **C)** Primary root length per number of nematodes inside the roots. **D)** Total secondary root length per number of nematodes inside the roots. **E)** Average secondary root length per number of nematodes inside the roots. Data from 2 independent biological repeats of the experiment were combined. The significance of differences between genotypes was calculated by analysis of variance (*n* = 14 to 18). Gray area indicates the 95% CI of the LOESS fit. Threshold for significance *P* < 0.05.

based on which we estimated the tolerance limit for *35S:WOX11-SRDX* at P_i = 2.25 (95% CI: 0.67 to 3.83) and for wild-type Col-0 at P_i = 4.84 (95% CI: 3.8 to 5.89). This difference in tolerance limits led us to conclude that WOX11 modulates the tolerance of *Arabidopsis* to cyst nematode infections.

Discussion

Excessive root branching is a classical symptom of nematode disease in plants of which the underlying causes nor the functions are well understood. Recently, we showed that endoparasitic cyst nematodes activate a JA-dependent damage signaling pathway leading to local auxin biosynthesis and subsequent de novo formation of secondary roots near infection sites (Guarneri et al. 2023). At the outset of this study, it was not clear if nematode-induced secondary roots emerge

from primary roots following the canonical auxin-dependent pathway for the formation of acropetal lateral roots or if they emerge following a different pathway. Our current data support the alternative hypothesis wherein the emergence of secondary roots in response to nematode damage follows the noncanonical WOX11-dependent pathway leading to the formation of adventitious lateral roots. This induction of adventitious lateral roots near nematode infection sites compensates for the inhibition of primary root growth by root-feeding cyst nematodes. We further show that the WOX11-mediated plasticity of root system architecture contributes to the tolerance of *Arabidopsis* to cyst nematode infections.

Our observations demonstrate that WOX11 modulates de novo root organogenesis near cyst nematode infection sites. Both WOX11- and ARF7/ARF19-mediated rooting pathways
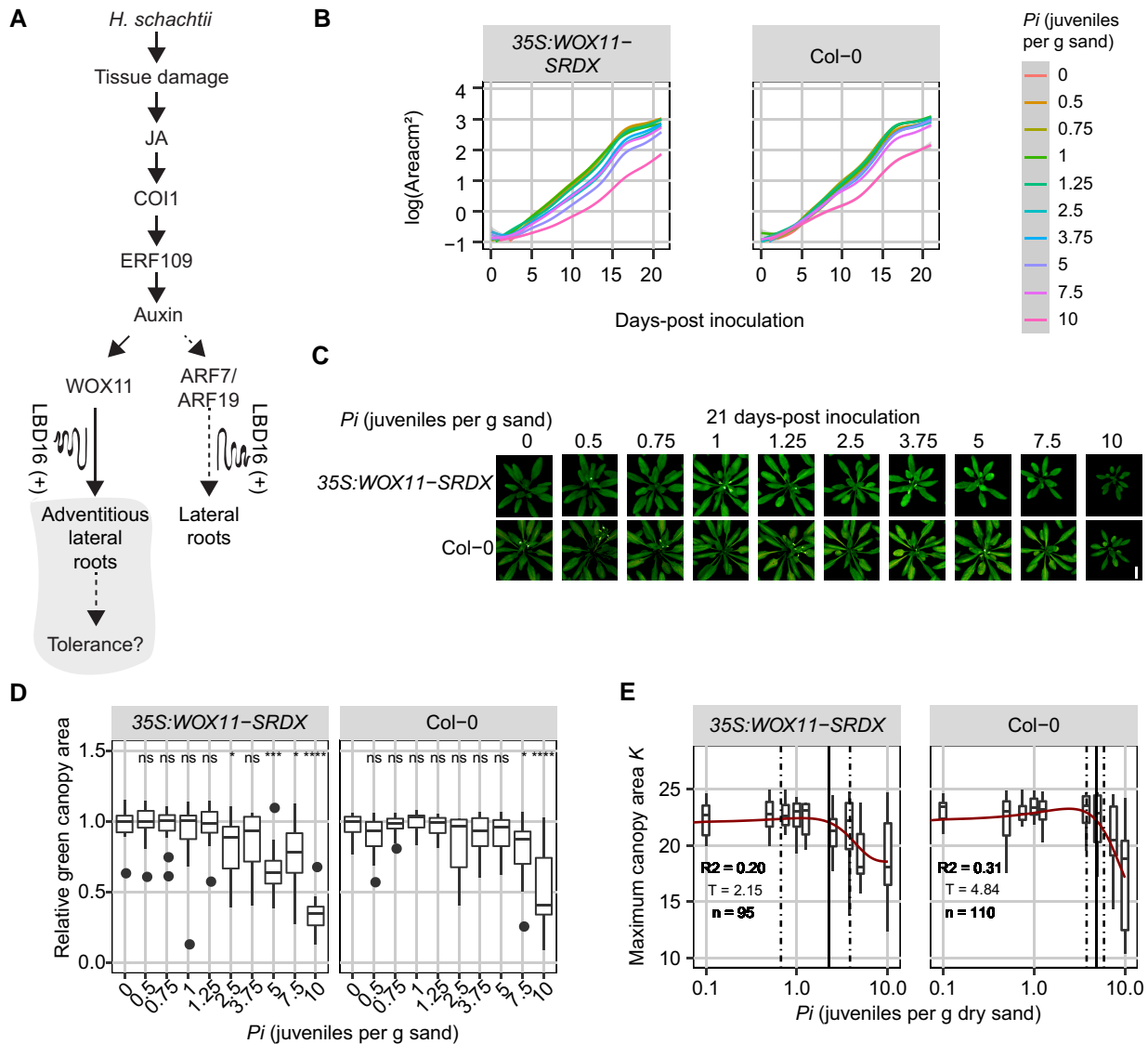
Figure 5. WOX11 is involved in tolerance to cyst nematode infection. **A)** Schematic diagram of *H. schachtii-* and WOX11-mediated adventitious lateral root emergence. Highlighted area indicates the tested part of the pathway. Curling line and "+" indicate the involvement of multiple proteins, including LBD16. Nine-day-old *Arabidopsis* seedlings were inoculated with 10 densities (P_i) of *H. schachtii* juveniles (0 to 10 J2s per g dry sand) in 200-mL pots containing 200 g of dry sand. **B)** Average growth curve of *Arabidopsis* plants inoculated with different inoculum densities of *H. schachtii* from 0 to 21 dpi. Line fitting was based on a LOESS regression. **C)** Representative images of plants inoculated with *H. schachtii* at 21 dpi. Images were digitally extracted for comparison. Scale bar: 1 cm. **D)** Relative green canopy area at 21 dpi. For the relative green canopy area, all values were normalized to the median of the measurements of the corresponding mock-inoculated plants. Data were analyzed with a Wilcoxon rank sum test; ns = not significant, *$P < 0.05$, **$P < 0.01$, and ***$P < 0.001$ ($n = 10$ to 18 plants per treatment). **E)** The maximum canopy area K per inoculation density of *H. schachtii*. The fitted line is from a Gaussian curve. Solid line indicates the tolerance limit. Dashed line indicates the CI. R^2 is the goodness of the fit, T is the tolerance limit, and n is the number of plants used for fitting the data. For boxplots, the horizontal line represents the median, the whiskers indicate the maximum/minimum range, and the black dots represent the outliers (1.5 times the interquartile range).

are activated by auxin, but they form a divergence point in the differentiation of adventitious lateral root primordia from lateral root primordia. WOX11 responds to auxin signals brought about by external cues, such as wounding (Sheng et al. 2017), and mediates tissue repair and regeneration mechanisms (Liu et al. 2014). In contrast, the auxin signals activating ARF7/ARF19 are thought to be developmentally regulated following endogenous rooting cues. Interestingly, both WOX11- and

ARF7/ARF19-mediated root organogenesis pathways converge on LBD16 (Okushima et al. 2007; Sheng et al. 2017; Zhang et al. 2023). Our findings indeed show that cyst nematodes induce expression of *LBD16* in a WOX11-dependent manner. However, this observation contradicts earlier work wherein *LBD16* expression was not observed in *Arabidopsis* infected with *H. schachtii* at similar time points after inoculation (Cabrera et al. 2014). It should be noted that we used a different

LBD16pro:LBD16-GUS reporter line containing a much larger genomic region upstream of *LBD16* (Sheng et al. 2017) compared to previous studies (Okushima et al. 2007; Cabrera et al. 2014). This extended promoter region included in the *LBD16pro:LBD16-GUS* line harbors multiple WOX11-binding sites, which are absent in previously used *LBD16-GUS* reporter lines and which may thus explain the differences in observed *LBD16* expression in cyst nematode-infected *Arabidopsis* roots.

Our data further show that both COI1 and ERF109 modulate WOX11 expression in response to cyst nematode infection, which positions WOX11 downstream of ERF109 within the JA-dependent damage signaling pathway. JA-dependent damage signaling induces local auxin biosynthesis, which drives the production of secondary roots (Guarneri et al. 2023). Auxin has been shown to directly activate *WOX11* expression, and as such WOX11 connects stress-induced auxin signaling to the establishment of adventitious lateral root founder cells (Sheng et al. 2017). ERF109 most likely modulates WOX11 activity by regulating local YUCCA-mediated biosynthesis of auxin (Cai et al. 2014). However, even in the absence of ERF109 (i.e. *erf109* mutant), we observed some *WOX11-GFP* expression in nematode infection sites. This agrees with our earlier observations demonstrating that besides damage-induced local biosynthesis of auxin, auxin transported from the shoots toward nematode infection sites also contributes to local stress-induced auxin maxima (Guarneri et al. 2023). WOX11 may thus integrate local and systemic auxin-based stress response mechanisms leading to the formation of adventitious lateral roots in nematode-infected *Arabidopsis*.

In our in vitro bioassays, WOX11 affected the number of secondary roots emerging from nematode-infected primary roots, but not the average secondary root length. Furthermore, we found that WOX11-mediated adventitious rooting compensated for the inhibition of primary root growth due to nematode infections, which implies that WOX11 mitigates the impact of nematode infections by adapting root system branching. This fits in the current model of wound-induced formation of secondary roots, wherein the activation of WOX11 initiates the cell fate transition of protoxylem cells into adventitious root founder cells (Liu et al. 2014). WOX11 is thought to be specific for adventitious root founder cells, where it activates, together with its homolog WOX12, LBD16- and WOX5-mediated divisions to initiate the formation of adventitious root primordia (Liu et al. 2014; Hu and Xu 2016). During these divisions, the expression of *WOX11* decreases, because of which it affects the number of secondary roots but is less likely to alter secondary root growth.

Based on the green canopy area as a proxy for measuring the overall impact of belowground stress on plant fitness, we conclude that WOX11-mediated root system plasticity also contributes to the tolerance of *Arabidopsis* to cyst nematode infections. The estimated tolerance limit of *35S:WOX11-SRDX* plants for cyst nematode infections was substantially lower than that of wild-type Col-0 plants. Others have shown that homologs of *Arabidopsis* WOX11 in rice, apple (*Malus*), and poplar enhance plant tolerance to abiotic stresses, such as drought and low nitrate conditions, by regulating adventitious lateral root formation (Cheng et al. 2016; Wang et al. 2020, 2021; Tahir et al. 2022). Furthermore, WOX11 functions as a key regulator in the regeneration of primary roots after mechanical injury by inducing the formation of adventitious lateral roots at the cut site (Sheng et al. 2017). Our study provides evidence of WOX11-mediated mitigation of the impact of belowground biotic stress.

WOX11-mediated adventitious rooting may contribute to tolerance of *Arabidopsis* to biotic stress by restoring the capacity of the root system to take up and transport water and minerals. Cyst nematodes modify host cells within the vascular cylinder into a permanent feeding structure, which interrupts the continuity of surrounding xylem vessels (Golinowski et al. 1996; Sobczak et al. 1997; Levin et al. 2020). As cyst nematodes develop, their feeding structures expand, consuming a larger part of the vascular cylinder while further impeding the flow of water and minerals (Bohlmann and Sobczak 2014). This is the reason why aboveground symptoms of cyst nematodes infections are often confused for drought stress. Local and systemic auxin-based stress signals may thus activate WOX11-mediated adventitious lateral rooting to maintain the flow of water and minerals to the xylem vessels above infection sites (Levin et al. 2020). At lower inoculation densities, WOX11-meditated adventitious lateral root formation from cyst nematode-infected primary roots may suffice to sustain normal *Arabidopsis* development and growth resulting in a more tolerant phenotype.

Recent research suggests that the cellular processes targeted by the transcriptional activity of WOX11 include the modulation of reactive oxygen species (ROS) homeostasis. In poplar, PagWOX11/12a has been shown to regulate the expression of enzymes involved in scavenging ROS under salt stress conditions (Wang et al. 2021). In crown root meristem cells of rice, WOX11 modulates ROS-mediated post-translational modifications (i.e. protein acetylation) of proteins required for crown root development (Xu et al. 2023). ROS are required for the induction of adventitious root formation from *Arabidopsis* explants (Shin et al. 2022). There is also evidence that ROS modulate auxin levels during the initiation of adventitious roots from *Arabidopsis* explants (Huang et al. 2020). Moreover, we have recently linked tolerance of *Arabidopsis* to cyst nematode infections, ROS-mediated processes, and root system plasticity (Willig et al. 2022). However, further research is needed to investigate if WOX11 influences ROS-related processes, or vice versa, in infection sites of cyst nematodes in *Arabidopsis* roots, and if such a mechanism plays a role in WOX11-mediated root plasticity and tolerance to nematode infections.

Materials and methods

Plant material and culturing
The *Arabidopsis* (*A. thaliana*) lines wild-type Col-0 (N60.000), *35S:WOX11-SRDX/arf7-1/19-1*, *arf7-1/19-1*, *LBD16pro:LBD16-GUS* and *35S:WOX11-SRDX/LBD16pro:LBD16-GUS* (Sheng

et al. 2017), *pWOX11::GFP*, *pWOX11::GFP-coi1-2*, *pWOX11::GFP-erf109*, *coi1-2*, and *erf109* were used. For in vitro experiments, seeds were vapor sterilized for 3 to 4 h using a mixture of hydrochloric acid (25% *v/v*) and sodium hypochlorite (50 g/L). Finally, sterile seeds were stratified for 4 days at 4 °C, after which they were sown on square Petri dishes (120 × 120 mm) containing modified Knop medium (Sijmons et al. 1991) in a growth chamber with a 16-h-light/8-h-dark photoperiod at 21 °C. For in vivo pot experiments, seeds were stratified for 4 d and sown on silver sand in 200-mL pots. Seedlings were grown at 19 °C and 16-h-light/8-h-dark conditions with LED light (150 lumens), as previously described in (Willig et al. 2023).

Hatching and sterilization of *H. schachtii*

H. schachtii cysts (Woensdrecht population from IRS, the Netherlands) were separated from the sand of infected *Brassica oleracea* plants as previously described (Baum et al. 2000). Cysts were transferred into a clean Erlenmeyer containing water with sodium azide (0.02% *w/v*). This mixture was gently stirred for 20 min. Later, sodium azide was removed by washing with tap water. Cysts were then incubated for 4 to 7 d in a solution containing 1.5-mg/mL gentamycin sulfate, 0.05-mg/mL nystatin, and 3 mM $ZnCl_2$. Hatched J2s were purified by centrifugation on a sucrose gradient (35% *w/v*), transferred to a 2-mL eppendorf tube, and surface sterilized for 15 min in a solution containing 0.16 mM $HgCl_2$, 0.49 mM NaN_3, and Triton X-100 (0.002% *v/v*). After washing the J2s 3 times with sterile tap water, *H. schachtii* J2s were resuspended in a sterile Gelrite (0.7% *w/v*, Duchefa Biochemie, Haarlem, the Netherlands) solution. A similar concentration of Gelrite solution was used as a mock treatment.

For in vivo pot experiments, J2s were hatched and collected in a similar way as described above. Nonsterile J2s were purified by centrifugation on a sucrose gradient (35% *w/v*) and washed 3 times with tap water. Nematodes were resuspended in tap water for specific inoculation densities.

Quantifying root system architecture of nematode-infected *Arabidopsis*

Seven-day-old *35S:WOX11-SRDX/arf7-1/19-1* and *arf7-1/19-1 Arabidopsis* seedlings were inoculated with either 90 *H. schachtii* J2s or a mock solution. Root architecture was inspected at 7 dpi using an Olympus SZX10 binocular with a 1.5× objective and 2.5× magnification. Scans were made of whole seedlings using an Epson Perfection V800 photo scanner. Pictures of nematode infections were taken with an AxioCam MRc5 camera (Zeiss) and the ZEN 3.2 blue edition software (Zeiss).

Nine-day-old *35S:WOX11-SRDX* and wild-type Col-0 seedlings, grown on 120 × 120 mm square Petri dishes were inoculated with 0 (mock), 0.5, 1.0, 2.5, 5.0, and 7.5 *H. schachtii* J2s per milliliter of modified Knop medium as previously described (Guarneri et al. 2023). Inoculations were done with two 5-*µ*L drops that were pipetted at opposite sides of

each seedling while keeping the Petri dishes vertical. At 7 dpi, scans were made of whole seedlings using an Epson Perfection V800 photo scanner. The architecture (i.e. total root length, primary root length, and total secondary root length) was measured using the WinRHIZO package for *Arabidopsis* (WinRHIZO pro2015, Regent Instrument Inc., Quebec, Canada). The number of root tips was counted manually based on the scans.

Acid fuchsine staining of nematodes

Nematodes within the roots were stained with acid fuchsin and counted as previously described (Warmerdam et al. 2018). For comparisons between genotypes, the background effect of the mutation on the root architecture was corrected by normalizing each measured root architecture component in infected seedlings to the median respective component in mock-inoculated roots.

Histology and brightfield microscopy

Four-day-old *Arabidopsis* seedlings were inoculated with 20 *H. schachtii* J2s or a mock solution. For histochemical staining of GUS activity, seedlings were incubated in a GUS staining solution (1 mg/mL X-GlcA in 100 mM phosphate buffer pH 7.2, 2 mM potassium ferricyanide, 2 mM potassium ferrocyanide, and Triton X-100 [0.2% *v/v*]) at 37 °C (Zhou et al. 2019) for 3 h. Stained seedlings were mounted in a chloral hydrate clearing solution (12 M chloral hydrate, glycerol [25% *v/v*]) and inspected with an Axio Imager nM2 light microscope (Zeiss) via a 20× objective. Differential interference contrast images were taken with an AxioCam MRc5 camera (Zeiss) and the ZEN 3.2 blue edition software (Zeiss).

Confocal laser microscopy of single *H. schachtii* infection sites

Four-day-old *Arabidopsis* seedlings were inoculated with roughly 5 sterile *H. schachtii* J2s in 10-*µ*L Gelrite (0.7% *w/v*). Single-nematode infection sites were selected for observation at 2, 3, 4, and 7 dpi. Infection sites were inspected using a Zeiss LSM 710 confocal laser scanning microscope and a 40× objective. After a single infection site was located, a Z-stack of 10 13 *µ*m-slices was made. Z-stacks were taken using the ZEN 2009 software (Zeiss). The imaging settings in ZEN 2009 were as follows: laser 488 at 50%, pinhole 41.4 *µ*m, enhanced green fluorescent protein (eGFP) 645 nm, and transmitted light detector (TPMT) 217 nm. Z-stacks were processed with ImageJ version 1.53 to quantify the fluorescence integrated density.

The postprocessing in ImageJ of 1 individual image was as follows: First, an auto-scaled compressed-hyper-Z-stack was created of the 10 layers made with the confocal microscope by using the Z-compression function at max intensity (Supplementary Fig. S4). Second, a duplicate of the original Z-stack was created, and a Gaussian filter with a sigma value of 2.0 was applied to this duplicate. This duplicate was subtracted from the original image by using the image calculator

function. Third, the image threshold limits were set to a specific range ranging from 0 to 100 depending on the quality of the image. The same threshold limits were applied to all images that were taken on the same day. Lastly, the particles were analyzed using Analyze Particles at size 0 to infinity and circularity 0.00 to 1.00.

High-throughput analysis of the green canopy area of nematode-infected *Arabidopsis* plants

Plants were imaged and analyzed as previously described (Willig et al. 2023). Prior to sowing, pots were filled with silver sand, covered with black coversheets, and were watered with Hyponex (1.7 mM/L NH_4^+, 4.1 mM/L K^+, 2 mM/L Ca_2^+, 1.2 mM/L Mg_2^+, 4.3 mM/L NO_3^-, 3.3 mM/L SO_4^{2-}, 1.3 mM/L $H2PO_4^-$, 3.4 μm/L Mn, 4.7 μm/L Zn, B 14 μm/L, 6.9 μm/L Cu, 0.5 μm/L Mo, 21 μm/L Fe, and pH 5.8) for 5 min. Seven days after sowing, seedlings were watered again for 5 min. Nine-day-old seedlings were inoculated with increasing densities of *H. schachtii* (0 to 10 juveniles per g dry sand). For our experiments, we did not use a blocking design as it would greatly increase the chance for error when manually inoculating plants. Every hour, pictures were taken of the plants (15 pictures/day) for a period of 21 d. At the end of the experiment, color corrections were done using Adobe Photoshop (version 22.5.6 20220204.r.749 810e0a0 ×64). The surface area of the rosette was determined using a custom-written ImageJ macro (ImageJ 1.51f; Java 1.8.0_321 [32-bit]), and Java was used to make GIFs.

Plant growth analysis and tolerance modeling using a high-throughput phenotyping platform

To analyze the growth data of the plants obtained from the high-throughput platform, we followed the same approach and used the same functions as in our previously published analytical pipeline (Willig et al. 2023), available via GitLab: https://git.wur.nl/published_papers/willig_2023_camera-setup.

In short, the measurement used was the median daily leaf area (cm^2), calculated from the 15 daily measurements. We used log_2-transformed data, where the rate of growth was determined per day per plant by (equation 1):

$$R_{x,t} = \log_2 (A_{x, t-1} - A_{x, t}),$$

where $R_{x,t}$ is the transformed growth rate of plant x at day t from day t_{-1} to day t based on the median green canopy area $A_{x,t}$.

The tolerance limit was modeled using a previously described method based on fitting growth models (Willig et al. 2023). Here, we fitted a logistic growth model using the *growthrates* package on the median daily leaf area A_t (cm^2) (equation 2):

$$A_t = \frac{K \times A_0}{A_0 + (K - A_0) \times e^{(-r \times t)}},$$

where K is the maximum green canopy area (cm^2), A_0 is the initial canopy area (cm^2), and r is the intrinsic growth rate (d^{-1}), which were determined as a function of time t (d) ($P < 0.1$).

Based on the relation between K and density, we could identify the tolerance limit (equation 3):

$$K = K_B + \frac{K_\sigma}{P_\sigma} \times e^{-\left(\frac{P_i - P_M}{P_\sigma}\right)^2},$$

where P_i is the initial nematode density in nematodes per gram soil, K_B is the basal canopy size, K_σ is the normalized maximum canopy area that can be achieved over the P_i range, P_σ is the deviation around the nematode density allowing maximum growth, and P_M is the nematode density at which maximum growth is achieved. We modeled the parameter values using *nls* and extracted CIs using the *nlstools* package (Baty et al. 2015). The tolerance limit (T_e), $2 * P_M$, was determined as described in Willig et al. (2023).

Statistical analyses

Statistical analyses were performed using the R software version 3.6.3 (Windows, ×64). The R packages used are *tidyverse* (https://CRAN.R-project.org/package=tidyverse), *ARTool* (https://CRAN.R-project.org/package=ARTool), and *multcompView* (https://CRAN.R-project.org/package=multcompView). The correlation between variables was calculated using the Spearman rank-order correlation coefficient. For binary data, the significance of the differences between proportions was calculated by a pairwise Z-test. For normally distributed data, the significance of the differences among means was calculated by ANOVA followed by Tukey's honestly significant difference (HSD) test for multiple comparisons. A nonparametric pairwise Wilcoxon test followed by false discovery rate correction for multiple comparisons was used for data with other distributions and 1 grouping factor. For the high-throughput platform data, we used the Wilcoxon test as implemented in the *ggpubr* package (https://cran.r-project.org/web/packages/ggpubr/index.html). The CI of the inoculum density-response curves was calculated by locally estimated scatterplot smoothing (LOESS) regression (as per default in *geom_smooth*) in R.

Author contributions

J.-J.W., N.G., J.B., and G.S. conceived the project. J.-J.W., N.G., T.v.L., S.W., I.E.A.-E. designed and performed the experiments. M.G.T. provided scripts for SYLM analysis. Data analysis was designed analyzed and interpreted by J.-J.W., N.G., and M.G.S. J.-J.W., N.G., and G.S. wrote the article. V.W. performed crosses of *coi1-2*, *erf109* with wild-type plants expressing *pWOX11::GFP*. V.W. and L.X. provided *Arabidopsis* mutant and reporter lines. V.W., L.X., A.G., M.G.S., and J.L.L.-T. provided critical feedback on the manuscript. All co-authors provided input for the submitted version.

Supplementary data

The following materials are available in the online version of this article.

Supplementary Figure S1. Primordia formed in response to *H. schachtii* infection in *arf7-1/19-1* mutant seedlings.

Supplementary Figure S2. Root architecture comparison between *35S:WOX11-SRDX* seedlings and wild-type Col-0 seedlings.

Supplementary Figure S3. COI1 and ERF109 contribute to *WOX11* expression upon *H. schachtii* infection.

Supplementary Figure S4. Noise removal process using Gaussian blur option in ImageJ.

Supplementary Figure S5. Adventitious lateral roots increase the total secondary root length upon nematode infection.

Supplementary Figure S6. Growth rates of *coi1-2*, *erf109*, and *35S:WOX11-SRDX* and wild-type Col-0 plants over time.

Supplementary Figure S7. Growth rates of *coi1-2*, *erf109*, and *35S:WOX11-SRDX* plants are more affected during *H. schachtii* than wild type.

Funding

Conflict of interest statement. The authors declare no conflict of interest.

Data availability

The data, including plant material, supporting this study's findings are available from the corresponding author upon request.

References

Baty F, Ritz C, Charles S, Brutsche M, Flandrois J-P, Delignette-Muller M-L. A toolbox for nonlinear regression in R: the package nlstools. J Stat Softw. 2015:**66**(5):1–21. https://doi.org/10.18637/jss.v066.i05

Baum TJ, Wubben MJ, Hardyy KA, Su H, Rodermel SR. A screen for Arabidopsis thaliana mutants with altered susceptibility to Heterodera schachtii. J Nematol. 2000:**32**:166–173.

Bebber DP, Holmes T, Gurr SJ. The global spread of crop pests and pathogens. Glob Ecol Biogeogr. 2014:**23**(12):1398–1407. https://doi.org/10.1111/geb.12214

Bohlmann H, Sobczak M. The plant cell wall in the feeding sites of cyst nematodes. Front Plant Sci. 2014:**5**:89. https://doi.org/10.3389/fpls.2014.00089

Cabrera J, Fernando ED, Melillo T, Fukaki H, Cabello S, Hofmann J, Fenoll C, Escobar C, Díaz-Manzano FE, Sanchez M, et al. A role for LATERAL ORGAN BOUNDARIES-DOMAIN 16 during the interaction Arabidopsis–Meloidogyne spp. provides a molecular link between lateral root and root-knot nematode feeding site development. New Phytol. 2014:**203**(2):632–645. https://doi.org/10.1111/nph.12826

Cai X-T, Xu P, Zhao P-X, Liu R, Yu L-H, Xiang C-B. *Arabidopsis* ERF109 mediates cross-talk between jasmonic acid and auxin biosynthesis during lateral root formation. Nat Commun. 2014:**5**:5833. https://doi.org/10.1038/ncomms6833

Cheng S, Zhou D-X, Zhao Y. WUSCHEL-related homeobox gene WOX11 increases rice drought resistance by controlling root hair formation and root system development. Plant Signal Behav. 2016:**11**(2):e1130198. https://doi.org/10.1080/15592324.2015.1130198

Fukaki H, Tasaka M. Hormone interactions during lateral root formation. Plant Mol Biol. 2009:**69**(4):437–449. https://doi.org/10.1007/s11103-008-9417-2

Gheysen G, Mitchum MG. How nematodes manipulate plant development pathways for infection. Curr Opin Plant Biol. 2011:**14**(4):415–421. https://doi.org/10.1016/j.pbi.2011.03.012

Golinowski W, Grundler FMW, Sobczak M. Changes in the structure of *Arabidopsis thaliana* during female development of the plant-parasitic nematode *Heterodera schachtii*. Protoplasma. 1996:**194**(1-2):103–116. https://doi.org/10.1007/BF01273172

Goverse A, Overmars H, Engelbertink J, Schots A, Bakker J, Helder J. Both induction and morphogenesis of cyst nematode feeding cells are mediated by auxin. Mol Plant-Microbe Interact 2000:**13**(10):1121–1129. https://doi.org/10.1094/MPMI.2000.13.10.1121

Guarneri N, Willig J-J, Sterken MG, Zhou W, Hasan MS, Sharon L, Grundler FMW, Willemsen V, Goverse A, Smant G, et al. Root architecture plasticity in response to endoparasitic cyst nematodes is mediated by damage signaling. New Phytol. 2023:**237**(3):807–822. https://doi.org/10.1111/nph.18570

Hiratsu K, Matsui K, Koyama T, Ohme-Takagi M. Dominant repression of target genes by chimeric repressors that include the EAR motif, a repression domain, in *Arabidopsis*. Plant J. 2003:**34**(5):733–739. https://doi.org/10.1046/j.1365-313X.2003.01759.x

Hoth S, Schneidereit A, Lauterbach C, Scholz-Starke J, Sauer N. Nematode infection triggers the de novo formation of unloading phloem that allows macromolecular trafficking of green fluorescent protein into syncytia. Plant Physiol. 2005:**138**(1):383–392. https://doi.org/10.1104/pp.104.058800

Hu X, Xu L. Transcription factors WOX11/12 directly activate *WOX5/7* to promote root primordia initiation and organogenesis. Plant Physiol. 2016:**172**(4):2363–2373. https://doi.org/10.1104/pp.16.01067

Huang A, Wang Y, Liu Y, Wang G, She X. Reactive oxygen species regulate auxin levels to mediate adventitious root induction in *Arabidopsis* hypocotyl cuttings. J Integr Plant Biol. 2020:**62**(7):912–926. https://doi.org/10.1111/jipb.12870

Jones JT, Haegeman A, Danchin EGJ, Gaur HS, Helder J, Jones MGK, Kikuchi T, Manzanilla-López R, Palomares-Rius JE, Wesemael WML, et al. Top 10 plant-parasitic nematodes in molecular plant pathology. Mol Plant Pathol. 2013:**14**(9):946–961. https://doi.org/10.1111/mpp.12057

Levin KA, Tucker MR, Bird DMK, Mather DE. Infection by cyst nematodes induces rapid remodelling of developing xylem vessels in wheat roots. Sci Rep. 2020:**10**(1):9025. https://doi.org/10.1038/s41598-020-66080-z

Liu J, Sheng L, Xu Y, Li J, Yang Z, Huang H, Xu L. *WOX11* and *12* are involved in the first-step cell fate transition during de novo root organogenesis in *Arabidopsis*. Plant Cell. 2014:**26**(3):1081–1093. https://doi.org/10.1105/tpc.114.122887

Liu R, Wen S-S, Sun T-T, Wang R, Zuo W-T, Yang T, Wang C, Hu J-J, Lu M-Z, Wang L-Q. PagWOX11/12a positively regulates the PagSAUR36 gene that enhances adventitious root development in poplar. J Exp Bot. 2022:**73**(22):7298–7311. https://doi.org/10.1093/jxb/erac345

Okushima Y, Fukaki H, Onoda M, Theologis A, Tasaka M. ARF7 and ARF19 regulate lateral root formation via direct activation of LBD/ASL genes in *Arabidopsis*. Plant Cell. 2007:**19**(1):118–130. https://doi.org/10.1105/tpc.106.047761

Olmo R, Cabrera J, Díaz-Manzano FE, Ruiz-Ferrer V, Barcala M, Ishida T, García A, Andrés MF, Ruiz-Lara S, Verdugo I, et al. Root-knot nematodes induce gall formation by recruiting developmental pathways of post-embryonic organogenesis and regeneration

to promote transient pluripotency. New Phytol. 2020:**227**(1): 200–215. https://doi.org/10.1111/nph.16521

Sheng L, Hu X, Du Y, Zhang G, Huang H, Scheres B, Xu L. Non-canonical WOX11-mediated root branching contributes to plasticity in *Arabidopsis* root system architecture. Development (Cambridge). 2017:**144**(17):3126–3133. https://doi.org/10.1242/dev.152132

Shin SY, Park S-J, Kim H-S, Jeon J-H, Lee H-J. Wound-induced signals regulate root organogenesis in *Arabidopsis* explants. BMC Plant Biol. 2022:**22**(1):133. https://doi.org/10.1186/s12870-022-03524-w

Sijmons PC, Grundler FMW, Mende N, Burrows PR, Wyss U. Arabidopsis thaliana as a new model host for plant-parasitic nematodes. Plant J. 1991:**1**:245–254.

Sobczak M, Golinowski W, Grundler FMW. Changes in the structure of *Arabidopsis thaliana* roots induced during development of males of the plant parasitic nematode *Heterodera schachtii*. Eur J Plant Pathol. 1997:**103**(2):113–124. https://doi.org/10.1023/A:1008609409465

Tahir MM, Tong L, Fan L, Liu Z, Li S, Zhang X, Li K, Shao Y, Zhang D, Mao J. Insights into the complicated networks contribute to adventitious rooting in transgenic MdWOX11 apple microshoots under nitrate treatments. Plant Cell Environ. 2022:**45**(10):3134–3156. https://doi.org/10.1111/pce.14409

van den Berg T, Korver RA, Testerink C, ten Tusscher KHWJ. Modeling halotropism: a key role for root tip architecture and reflux loop remodeling in redistributing auxin. Development (Cambridge). 2016:**143**(18):3350–3362. https://doi.org/10.1242/dev.135111

Wang L-Q, Li Z, Wen S-S, Wang J-N, Zhao S-T, Lu M-Z. WUSCHEL-related homeobox gene PagWOX11/12a responds to drought stress by enhancing root elongation and biomass growth in poplar. J Exp Bot. 2020:**71**(4):1503–1513. https://doi.org/10.1093/jxb/erz490

Wang L-Q, Wen S-S, Wang R, Wang C, Gao B, Lu M-Z. PagWOX11/12a activates PagCYP736A12 gene that facilitates salt tolerance in poplar. Plant Biotechnol J. 2021:**19**(11):2249–2260. https://doi.org/10.1111/pbi.13653

Warmerdam S, Sterken MG, van Schaik C, Oortwijn MEP, Sukarta OCA, Lozano-Torres JL, Dicke M, Helder J, Kammenga JE, Goverse A, et al. Genome-wide association mapping of the architecture of susceptibility to the root-knot nematode *Meloidogyne* incognita in *Arabidopsis thaliana*. New Phytol. 2018:**218**(2):724–737. https://doi.org/10.1111/nph.15034

Willig J-J, Guarneri N, van Steenbrugge JJM, de Jong W, Chen J, Goverse A, Lozano Torres JL, Sterken MG, Bakker J, Smant G. The *Arabidopsis* transcription factor TCP9 modulates root architectural plasticity, reactive oxygen species-mediated processes, and tolerance to cyst nematode infections. Plant J. 2022:**112**(4):1070–1083. https://doi.org/10.1111/tpj.15996

Willig J-J, Sonneveld D, van Steenbrugge JJM, Deurhof L, van Schaik CC, Teklu MG, Goverse A, Lozano-Torres JL, Smant G, Sterken MG. From root to shoot; quantifying nematode tolerance in *Arabidopsis thaliana* by high-throughput phenotyping of plant development. J Exp Bot. 2023:**74**(18):5487–5499. https://doi.org/10.1093/jxb/erad266

Xu Q, Wang Y, Chen Z, Yue Y, Huang H, Wu B, Liu Y, Zhou D-X, Zhao Y. ROS-stimulated protein lysine acetylation is required for crown root development in rice. J Adv Res. 2023:**48**:33–46. https://doi.org/10.1016/j.jare.2022.07.010

Zhang T, Ge Y, Cai G, Pan X, Xu L. WOX-ARF modules initiate different types of roots. Cell Rep. 2023:**42**(8):112966. https://doi.org/10.1016/j.celrep.2023.112966

Zhou W, Lozano-Torres JL, Blilou I, Zhang X, Zhai Q, Smant G, Li C, Scheres B. A jasmonate signaling network activates root stem cells and promotes Regeneration. Cell. 2019:**177**:942–956.e14.